INTL JOURNAL OF ELECTRONICS AND TELECOMMUNICATIONS, 2026, VOL. 72, NO. 3, PP. 1-9
Manuscript received December 21, 2024; revised June, 2026. doi: 10.24425/ijet.2026.1731

A comprehensive study of predictive models in electric power systems using Soft Starter and Variable Frequency Drive methods

Syamsir Alam, Lukman Medriavin Silalahi, Lidiya, and Imelda Uli Vistalina Simanjuntak

Abstract—**The focus of this research problem is the investigation of predictive models in electric power installation systems in an effort to develop New Renewable Energy (NRE) due to the challenge of depletion of fossil energy sources. This research proposes to investigate the deepening of education and training using the Soft-Starter (SS) and Variable Frequency Drive (VFD) methods to produce efficiency and optimize the reliability of the electrical system. This investigation took information from the results of a technical study using ETAP. The results show that the use of a transformer with a capacity of 630kVA produces a 3-phase induction motor load of 534.5kW. Furthermore, the success of the SS method in reducing the surge during the start phase is 3.25 times the full load current, previously without the SS method is 5.75 times the full load current. The improvement in energy efficiency is shown by a decrease in transformer load from 85.2% to 76.5% due to a decrease in power consumption of 58.22kW. Finally, the conclusions resulted in a predictive investigation of the power system that has successfully demonstrated operational reliability, power distribution optimization.**

Keywords—**Inverter SNV-GH3041; Public Street Lighting; Vertical Axis Wind Turbine; Wind Energy; Wind Power Plant**

I. INTRODUCTION

THE transformation of the energy sector towards sustainable and renewable energy has experienced a significant increase [1]. Based on the World Economic Forum Global Risk Report [2], [3] that climate change in the next 10 years is seen as the risk that poses the most long-term threat. The investigation was carried out on the electricity sector as the dominant contributor to emissions [4]–[6] namely efforts to use biomass as a sustainable fuel, by converting it from waste into electrical energy. The customer side adopts the energy efficiency embedded in electric motors as part of the mitigation measures by converting electrical energy into motion energy for production equipment. The use of electric motors causes global industrial electricity consumption to continue to increase, along with the increase in Greenhouse Gas Emissions (GGE) [7]–[9].

Furthermore, This impacts conductor cables that may not be able to handle high current loads. The issues that have been raised have an impact on the reliability of the overall electrical system. Therefore, the identification and characterization of decision-making factors for the efficient design of electrical systems is urgently needed [10]–[13].

Based on [14]–[16], the main factors driving the need for more efficient electric motors are due to the analysis of global market needs, energy efficiency policies, and rising electricity prices. This research uses an electric motor approach for technical, economic, and environmental analysis to evaluate the impact of new policies, including the Motor Drive Unit standard. Finally, these findings support policy changes for the electric motor market to be more sustainable in optimizing motor systems thereby increasing energy savings to 3100 TWh in the same year, with a reduction in carbon emissions by 469 Mton CO2eq by 2040.

According to [17]–[19] stated that the main need of the industry lies in electric motors in supporting the total load capacity of the industry. This has been carried out a study approach using numerical study calculations on voltage drops during motor starting, transformers on 11kV and 3.3kV buses and short-circuit power. The results of the starting motor analysis produced a comparison of voltage drop and short-circuit current between bus transformer voltages. Finally it was stated that any case of a motor connected to a low voltage bus would result in a voltage drop percentage above 15%. Furthermore, in the case of a motor connected to a high voltage bus if the percentage of voltage drop is less than 15%.

Based on [20], formulate capacitor allocation based on the determination of the location, type, and size of the capacitor as an optimization problem to improve the voltage profile and reduce power loss. The methodology applied to verify the effectiveness of the proposed algorithm. The simulation was tested against a test system of 34 similar buses. In the case without capacitors, the energy loss of the system is 1,215MWh. Meanwhile, the proposed capacitor placement algorithm can reduce energy loss by up to 883MWh.

The literature review that has been carried out is a collection of in-depth explanations regarding the calculation of electrical loads based on the classification of load types. Therefore, there is room for further investigation in detailing important aspects in the design of industrial electric power installation systems. Thus, this research proposes to investigate a predictive model in electric power installation systems using the Soft Starter (SS) and Variable Frequency Drive (VFD) methods. Especially in 3-phase induction motors with constant and variable load [21]–[23].

The first author is with Universitas Mercu Buana, Indonesia (email: syamsir.alam1@mercubuana.ac.id).
The second author is with Universitas Presiden, Indonesia (email: lukman.silalahi@president.ac.id).
The third and fourth authors are with Universitas Mercu Buana, Indonesia (email: lidiyaliya1@gmail.com, imelda.simanjuntak@mercubuaca.ac.id).

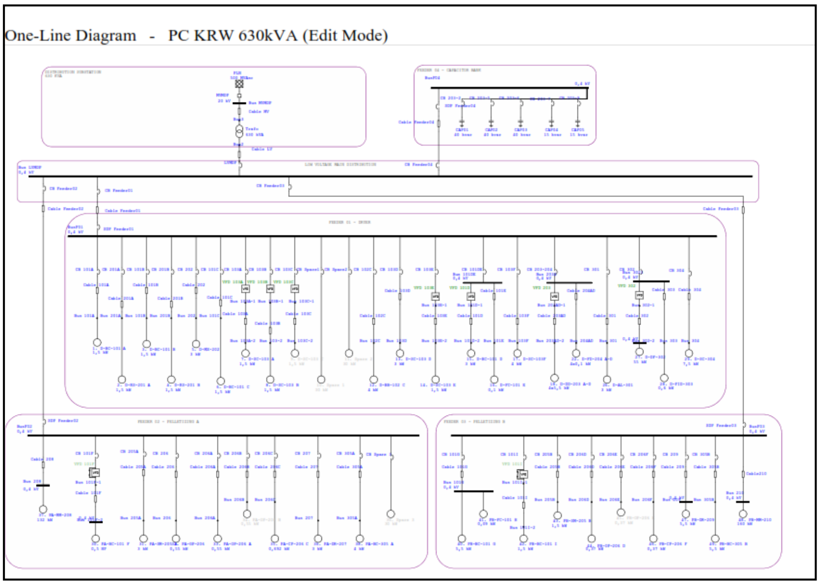

Fig. 1. *Single line diagram*

Factors such as voltage drop, power loss, and system reliability are the main focus of this research, further establishing a Single Line Diagram (SLD) design, the development of calculations on several constant and variable load conditions to verify the proposed design, until it is simulated until tested using ETAP software [24], [25]. It is expected that there will be optimization of power quality in addition to using VFD [26]–[29] and SS [30], also carried out through two other main approaches, namely increasing the power factor and cable selection.

The objective of this research is to design an electric power installation system using the SS method analysis based on the results of the investigation of the predictive model on the 3-phase induction motor starting system compared to the VFD method applied to the Direct On-Line (DOL) scheme to achieve power consumption savings and evaluate the efficiency and reliability of the system.

II. Method

Figure 1 shows the results of the design of the predictive model based on the function of each planned as follows:

1. Continues load (C), operated continuously. This load includes processes that require constant power availability to maintain smooth operations.
2. Intermittent load (I), operated periodically with operations is half the time.
3. Standby load (S), acts as a backup and is operated in a standby state with an operational factor of 0.1 or equivalent to 6 loads in this research. This load is activated when needed and supports the overall reliability of the operational system.

Table I indicates the information of the load on the feeder 01: dryer, each has a rated power of 101.1kW, 7.5kW, and 61.5kW and a total power rating of 179.1kW.

Table II indicates the information of the load on the feeder 01: pelletizer A, there are 6-units acting as a continuous load (C) with total load rated power of 142.92kW, 2-units acting as an intermittent load (I) with total load rated power of 1.24kW, and 2-units acting as a standby load (S) with total load rated power of 30.55 kW. Thus, the total power rating on pelletizer A is 174.7kW.

TABLE I
FEEDER LOAD DATA 01: DRYER

Item	kW	PF	η	Load Factor	Load Duty
Rotary screener 2	1,5	0,78	0,85	0,83	Intermittent load (I)
Mixer	3	0,95	0,85	0,83	Intermittent load (I)
Belt conveyor	1,5	0,78	0,85	0,83	Intermittent load (I)
Spare 1	30	0,86	0,91	0,91	Standby load (S)
Spare 2	30	0,86	0,91	0,91	Standby load (S)
Input conveyor	1,5	0,78	0,85	0,83	Continues load (C)
Rotary screener	1,5	0,78	0,85	0,83	Continues load (C)
Belt conveyor	1,5	0,78	0,85	0,83	Continues load (C)
Buttom Blower	4	0,88	0,85	0,83	Continues load (C)
Fuel air blower	3	0,85	0,85	0,83	Continues load (C)
Fuel Conveyor	1,5	0,77	0,853	0,83	Continues load (C)
Fan of conveyor	0,1	0,85	0,8	0,7	Continues load (C)
Drum dryer 1	5,5	0,82	0,877	0,83	Continues load (C)
drum dryer 2	5,5	0,82	0,877	0,83	Continues load (C)
drum dryer 3	5,5	0,82	0,877	0,83	Continues load (C)
drum dryer 4	5,5	0,82	0,877	0,83	Continues load (C)
Fan 1	0,1	0,82	0,8	0,7	Continues load (C)
Fan 2	0,1	0,82	0,8	0,7	Continues load (C)
Fan 3	0,1	0,82	0,8	0,7	Continues load (C)
Fan 4	0,1	0,82	0,8	0,7	Continues load (C)
Discharge machine	7,5	0,85	0,91	0,9	Continues load (C)

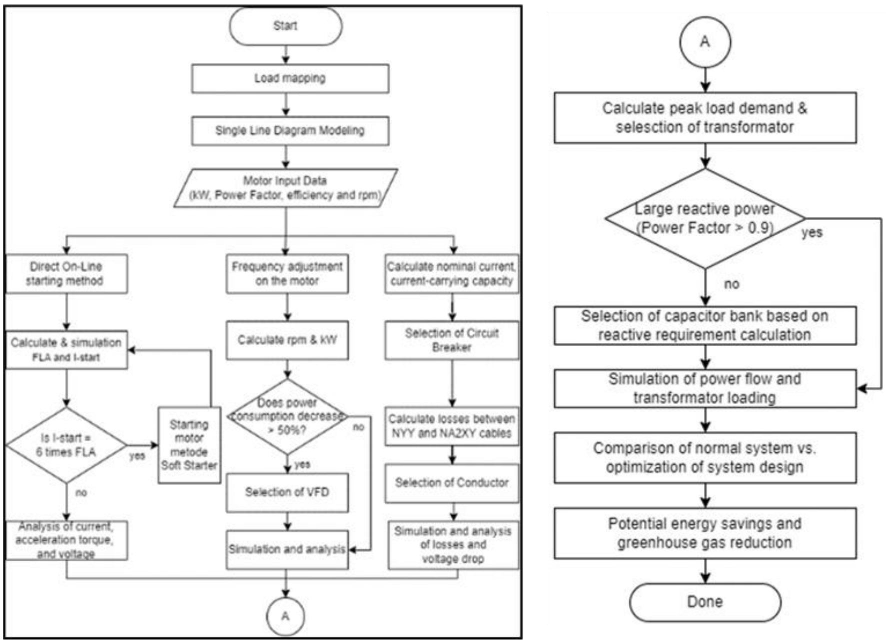

Fig. 2. *Flowchart design*

TABLE II
FEEDER LOAD DATA 02: PELLETIZER A

Load List	kW	PF	η	Load Factor	Load Duty
Feeding Conveyor	0,5	0,56	0,8	0,83	Continues load (C)
Kickout Motor	3	0,85	0,85	0,83	Continues load (C)
Grease Pump	0,55	0,77	0,85	0,75	Continues load (C)
Dust remover	3	0,85	0,8	0,83	Continues load (C)
Main Motor 1,5 tph	132	0,89	0,95	0,92	Continues load (C)
Pellet Conveyor	4	0,85	0,85	0,83	Continues load (C)
Lubricating pump 1	0,55	0,85	0,8	0,75	Intermittent load (I)
Water cooling pump	0,69	0,85	0,8	0,75	Intermittent load (I)
Lubricating pump 2	0,55	0,85	0,8	0,75	Standby load (S)
Spare 3	30	0,86	0,85	0,91	Standby load (S)

Furthermore, table III is the identification of the load on feeder 03: pelletizer B. Rated power of 179.59kW serves 7-units as a continuous load (C), rated power of 0.74kW serves 2-units as intermittent load (I), and 1-unit as standby load (S) with a rated power of 0.37kW. So, the total power rating is 180.7 kW. Thus, the total power rating on pelletizer B is 534.5kW.

TABLE III
FEEDER LOAD DATA 03: PELLETIZER B

Load List	kW	PF	η	Load Factor	Load Duty
Feeding conveyor	5,5	0,85	0,85	0,83	Continues load (C)
Feeding conveyor radiating	0,09	0,85	0,8	0,7	Continues load (C)
Input belt conveyor	1,5	0,85	0,78	0,83	Continues load (C)
Scraper motor	1,5	0,77	0,85	0,83	Continues load (C)
Dust Collector	5,5	0,85	0,85	0,83	Continues load (C)
Main Motor 2 tph	160	0,89	0,954	0,92	Continues load (C)
Pellet conveyor	5,5	0,85	0,85	0,83	Continues load (C)
Oil pump 1	0,37	0,85	0,8	0,75	Intermittent load (I)
Fan of oil cooling	0,37	0,85	0,8	0,75	Intermittent load (I)
Oil pump 2	0,37	0,85	0,8	0,75	Standby load (S)

Loads are divided into two main groups, including load data (power rating, cos phi, motor efficiency, speed) and load characteristics. Furthermore, it is collected for use in detailing the initial current using the SS method to ensure the reliability of the system based on the magnitude of the voltage drop at start.

Instead, frequency regulation uses the VFD method to calculate power and voltage to obtain the identification of potential energy savings. Next, analyze the selection of circuit breakers, conductors and transformers based on the calculation of maximum power, load current, nominal current, and current conductivity in each motor.

This research focuses on increasing the power factor to reduce losses in the system. Furthermore, this research was simulated using software known as ETAP. ETAP plays a role in simulating predictive models to validate design results, proving that the results of investigations on predictive models of electric power systems have improved reliability and resulted in significant energy savings.

The test was carried out using a comparison of two main motors with large capacity, namely the 1.5 tph main motor which has a power of 132 kW and the 2 tph main motor with a power of 160 kW using the SS method applied to the DOL scheme.

Figure 2 shows a flowchart of the research design that visually illustrates the sequence of stages. The first step involves identifying the load characteristics of the 49 3-phase induction motors used.

III. RESULT AND DISCUSSION

A. Soft Starter Method Testing

A common problem that must be considered is that when starting an induction motor, there will be a significant current surge of up to 6 times the nominal current. Based on data collection information, the motor is known to have a capacity of 132 kW, cosφ 0.89 and efficiency of 94.7%. The total starting current of the motor using the SS method is calculated as follows:

$$FLA = \frac{P}{\sqrt{3}\,V\cos\varphi} = \frac{132}{\sqrt{3}\ \times 0{,}38 \times 0{,}89} = 225{,}34A \qquad (1)$$

$$I_{before\ SS} = 6 \times FLA = 6 \times 225{,}34 = 1352{,}04A \qquad (2)$$

$$I_{after\ SS} = 6 \times 50\% \times FLA = 6 \times 50\% \times 225{,}34 = 676{,}02A \qquad (3)$$

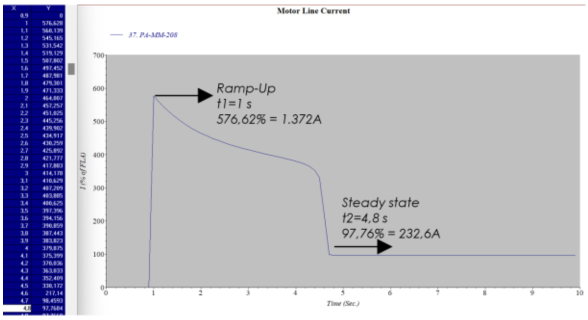

Fig. 3. Motor current versus time curve (SS method)

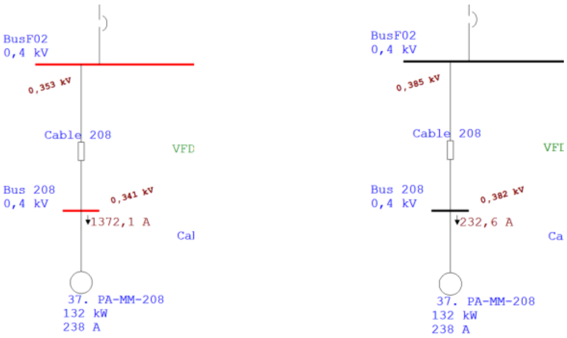

(a) **(b)**

Fig. 4. DOL simulation results on (a) t1=1 s (b) t2=4,8 s

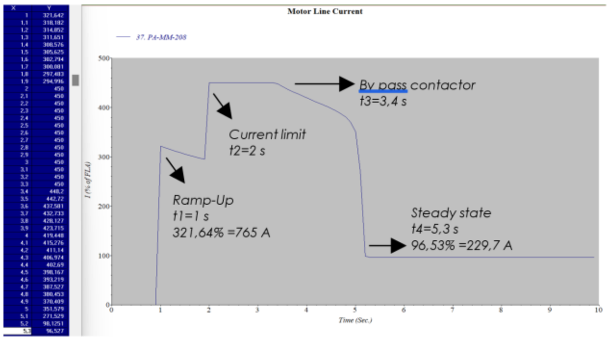

Fig. 5. Motor current versus time curve (SS method)

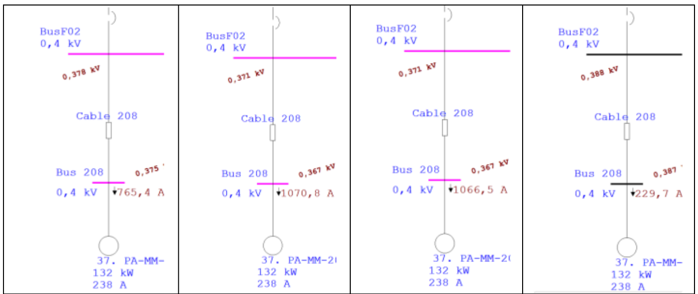

(a)	(b)	(c)	(d)

Fig. 6. SS simulation results on (a) t1=1 s (b) t2=2 s (c) t3=3,4 s (d) t4=5,3 s

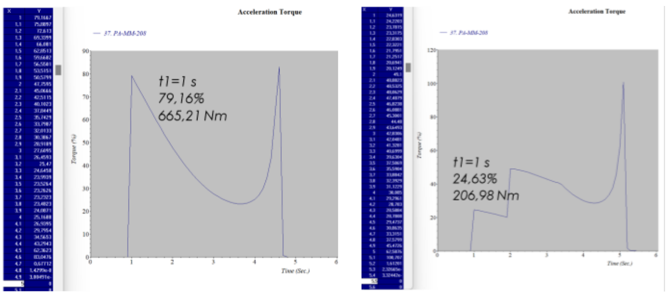

(a) (b)

Fig. 7. DOL simulation results on (a) t1=1 s (b) t2=4,8 s

Figure 3 is the result of the simulation of the DOL scheme, in figure 4a it is shown that there is an initial current surge of 1,372.1 A when t_1 = 1s because the motor directly obtains a full-time ramp up voltage. Figure 4b shows the normal condition or steady condition when t_2 = 4,8s a current of 232.6 A is obtained because it has reached its full speed. Furthermore, figure 5 is the simulation result using the SS method, this method shows that the Silicon Control Rectifier (SCR) as the SS constituent circuit successfully controls the motor voltage at the beginning of the ramp up process, slowly to the motor and does not cause high spikes, which is 321.64% of Full Load Ampere (FLA) or equivalent to 765.4 A shown in Figure 6a when t_1=1s. Then, switching to the normal setting state when t_3 = 3,4s, the motor resumes contactor bypass contact until the initial phase is completed when t_4=5,3s. Figure 6b shows a steady condition with a current of 229.7A. Furthermore, the SS circuit will be replaced by a bypass contactor during the run phase.

Figure 7 shows the acceleration torque which is the result of the difference between the torque of the motor and the torque of the load, meaning that the higher the torque obtained, the faster the acceleration of the motor. The amount of torque is calculated as follows.

$$T = \frac{60 \times P}{2\pi n} = \frac{60 \times 132000}{2 \times \pi \times 1500} = 840{,}34Nm \qquad (4)$$

$$T_{start-DOL} = 80\% \times T = 672{,}27Nm \qquad (5)$$

$$\frac{T_{start-SS}}{T} == \left(\frac{676{,}02}{1352{,}04}\right)^2 \times 840{,}34 = 210{,}08Nm \qquad (6)$$

It was analyzed that the results obtained were not so far compared to the simulation results. With the SS method, the motor requires a slower acceleration time of 5.5 seconds. So that the comparison of test results on both motors has the same properties, in detail can refer to table IV.

TABLE IV

TEST RESULTS OF SS METHOD

Item	Before SS-method			AfterSS-method		
	Calc	Simulate	%Error	Calc	Simulate	%Error
1.5tph main motor						
Starting current (A)	1352	1372	1,5	676	765	11,7%
Starting torque (Nm)	672	665	1,1	210	206	1,5%
V-bus (volt)		341		375		
V-drop		14,8%		6,3%		
2tph main motor						
Starting current (A)	1638	1643	0,3	819	940	12,9
Starting torque (Nm)	814	814	0,1	254	253	0,5
V-bus (volt)		332		380		
V-drop		17%		5%		

Based on equation 7 that the motor is operated without using the SS method, the initial current jumps an average of 5.75 times that of the FLA, resulting in a voltage drop of 14.8% and 17%. Furthermore, based on equation 8 that the motor has used the SS method produces an average starting current of 3.25 times that of FLA. The analysis obtained was that there was a decrease at the beginning of the torque movement, although there was a decrease in bus voltage, it was still within the permissible limit. Furthermore, the SS method protects the motor from damage and at the same time can extend the life of the motor as well as the entire system by reducing motor heating, reducing mechanical stress on the motor, and reducing the electrodynamic load on the power cable.

$$\overline{X_{before\ SS}} = \frac{(576{,}62 + 573{,}87)\%}{2} = 575\% = 5{,}75 \times FLA \quad (7)$$

$$\overline{X_{after\ SS}} = \frac{(321{,}64 + 328{,}48)\%}{2} = 325{,}08\% = 3{,}25 \times FLA \quad (8)$$

B. *Variable Frequency Drive Method Testing*

Under normal circumstances, the motor will provide maximum power. However, energy savings can be achieved if the speed of the motor can be reduced by changing the frequency in response to the load requirement when the load is reduced. For example, an induction fan motor is known that its capacity is 55 kW, 1485 rpm, cosφ 0.86 and efficiency 93.5% is calculated as follows:

$$n_s = \frac{120 \times f}{Pole} = \frac{120 \times 50}{4} = 1500rpm \quad (9)$$

$$Slip = \frac{(n_s - n_r)}{n_s} \times 100\% = \frac{(1500 - 1485)}{1500} \times 100\% = 1\% \quad (10)$$

$$n = f(1 - slip) = f(1 - 1\%) = 0{,}99frpm \quad (11)$$

$$n_{s(8Hz)} = n \times \frac{f_{8Hz}}{f_{50Hz}} \times n_s = 0{,}99 \times \frac{8Hz}{50Hz} \times 1500 = 237{,}6rpm \quad (12)$$

First, examination based on frequency and speed. The analysis suggests that speed is directly proportional to frequency although there is a difference due to slip. Therefore, the VFD method allows smoother than motor starting, also reducing the initial torque when the motor is started, thus reducing the slip in the initial phase.

$$P_{absorbed} = P_{rating} \times load\ factor = 55 \times 0{,}91 = 50{,}05kW \quad (13)$$

$$P_{out} = \frac{P_{absorbed}}{n} = \frac{50{,}1}{0{,}935} = 53{,}529kW \quad (14)$$

$$P = \omega \times T = \frac{2\pi n}{60} \times T \rightarrow P = n \times T \quad (15)$$

$$Percentage_{frequency} = \frac{f_{8Hz}}{f_{50Hz}} \times 100\% = \frac{8}{50} \times 100\% = 16\% \quad (16)$$

$$P_{16\%} = 16\% \times 2{,}6\% \times P_{out} == 0{,}22kW \quad (17)$$

The output power of the motor can be seen in equation 13-14. The output power at each frequency variation can be calculated by multiplying the torque and velocity while the required load torque is proportional to the speed squared shown in equations 15-16. This results in an output power value equivalent to 0.22 kW at the 8 Hz frequency shown in equation 17.

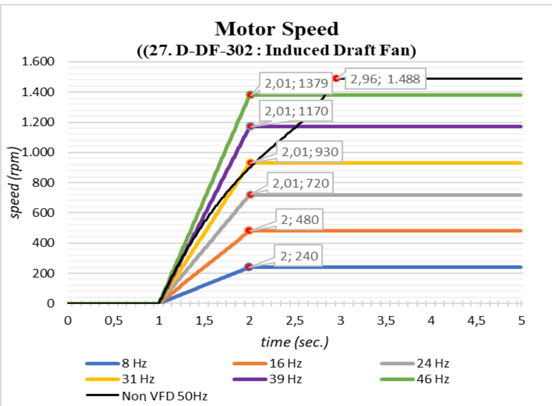

Fig. 8. Relationship curve between motor speed and time

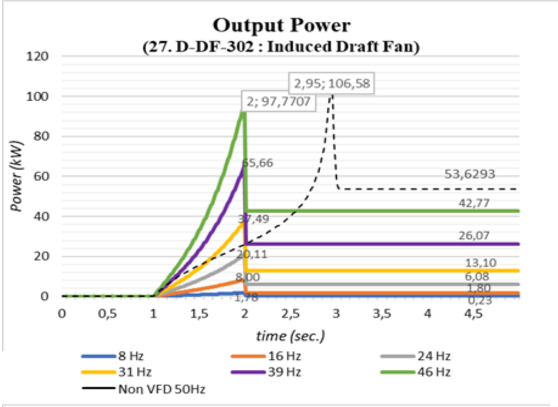

Fig. 9. Relationship curve between output power and time

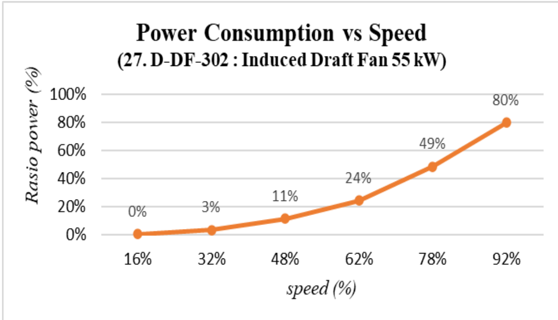

Fig. 10. Power consumption versus speed curve

Figure 8 is the simulation result of the motor speed that informs before/after implementing the VFD method. The black line is the motor speed before implementation of the VFD method, but the other line colors are the implementation of the VFD method. This analysis shows that the motor always operates at the maximum frequency of 50Hz and a speed of 1,488rpm. However, when load variation occurs, the average frequency is 27.33Hz, and the maximum speed of the motor is 820 rpm. Figure 9 shows the output power simulation. The black line is the output power result before implementing the VFD method and after implementing the VFD method. The difference between calculation and simulation is not so far, only between 2.55%-2.65%.

Figure 10 shows the power consumption to the speed curve. The motor operates at a maximum power of 53,629kW. But when the load fluctuates, the average frequency of the motor is 27.33Hz or the equivalent power is 15.01kW. This analysis shows an energy saving of 72% of the normal output power which refers to the relationship curve between power consumption and speed. Table V shows that the 9-unit load studied can save power by 56.22 kw or 63.56%. This shows the success of the VFD method in operating the motor at the ideal speed under any load condition.

C. *Electric Load Calculation*

Energy requirements are calculated based on parameter analysis, including power rating, absorbed load, consumed load which is influenced by the efficiency of the motor itself as shown in equation 18-20.

$$P_{absorbed} = P_{rating} \times load\ factor = 160 \times 0{,}92 = 147{,}2kW \quad (18)$$

$$P_{absorbed} = P_{consumed} = \frac{P_{absorbed}}{n} = \frac{147{,}2}{0{,}93} = 158{,}28kW \quad (19)$$

$$Q_{consumed} = P \times \sqrt{\frac{1}{(\cos\theta)^2} - 1} = 81{,}09kVAR \tag{20}$$

The results of the calculation of the electrical load on Feeder 01 based on table I produce a power consumption at a continuous load (C) of 106.7kW, an intermittent load (I) of 7.3kW, and a standby load (S) of 65.7kW. The results of the calculation of the electrical load on Feeder 02 based on table II produce a power consumption at a continuous load (C) of 139kW, an intermittent load (I) of 1.16kW, and a standby load (S) of 32.63kW. The results of the calculation of the electrical load on Feeder 03 based on table III produce a power consumption at a continuous load (C) of 173.4kW, an intermittent load (I) of 0.69kW, and a standby load (S) of 0.35kW. Then the results of the consumed load calculation on each feeder are used to determine Peak Load Demand (PLD) using formula $P_{PLD} = 100\%\, C + 50\%\, I + 10\%\, S$. Thus, the three groups are summed, including total peak power (P) of 433.6 kW, total reactive power (Q) of 240.5 kVAR, and apparent power (S) of 496.12 KVA.

1. Feeder 01: Dryer

$$P_{feeder\ 1} = P_{PLD} = (100\% \times 106{,}7) + (50\% \times 7{,}3) + (10\% \times 65{,}7) = 116{,}9kVA \tag{21}$$

$$Q_{feeder\ 1} = Q_{PLD} = (100\% \times 67{,}5) + (50\% \times 4{,}5) + (10\% \times 39{,}3) = 73{,}7kVA \tag{22}$$

$$S_{feeder\ 1} = S_{PLD} = \sqrt{(P_{PLD})^2 + (Q_{PLD})^2} = \sqrt{(116{,}9)^2 + (73{,}7)^2} = 138{,}20kVA \tag{23}$$

2. Feeder 02: Pelletizer A

$$P_{feeder\ 2} = P_{PLD} = (100\% \times 139) + (50\% \times 1{,}16) + (10\% \times 32{,}63) = 142{,}9kVA \tag{24}$$

$$Q_{feeder\ 2} = Q_{PLD} = (100\% \times 72{,}8) + (50\% \times 0{,}72) + (10\% \times 19{,}38) = 75{,}1kVA \tag{25}$$

$$S_{feeder\ 2} = S_{PLD} = \sqrt{(P_{PLD})^2 + (Q_{PLD})^2} = \sqrt{(142{,}9)^2 + (75{,}1)^2} = 161{,}41kVA \tag{26}$$

3. Feeder 03: Pelletizer B

$$P_{feeder\ 3} = P_{PLD} = (100\% \times 173{,}4) + (50\% \times 0{,}69) + (10\% \times 30{,}35) = 173{,}8kVA \tag{27}$$

$$Q_{feeder\ 3} = Q_{PLD} = (100\% \times 91{,}5) + (50\% \times 0{,}43) + (10\% \times 0{,}21) = 91{,}7kVA \tag{28}$$

$$S_{feeder\ 3} = S_{PLD} = \sqrt{(P_{PLD})^2 + (Q_{PLD})^2} = \sqrt{(173{,}8)^2 + (91{,}7)^2} = 196{,}51kVA \tag{29}$$

D. Capacity of Conductor Cable and Main Circuit Breaker

The determination of the cable cross-section size is based on the calculation of the Conducting Current (CC) according to General Requirements for Electrical Installations (GREI) which is 125% of the FLA. Meanwhile, the induced fan motor has a 1.5tph and 2tph. The main breaker of the feeder is carried out based on the comparison of power loss and voltage drop between two types of cables, namely NYY (Copper) and NA2XY (Aluminum). For example, the main motor of 1.5tph has an FLA value 225,34A and cos φ of 0,89 along 50m. From the overall calculation results that the NA2XY cable was finally chosen because of the lower power loss during the distribution process.

1. NYY 1x120 mm^2 cable, resistance value 0.153 ohm/km and reactance 0.091 ohm/km

$$R = \frac{0{,}153}{1000} \times 50 = 0{,}00765\Omega \tag{30}$$

$$X = \frac{0{,}091}{1000} \times 50 = 0{,}00455\Omega \tag{31}$$

$$P_{losses-NYY} = \sqrt{3} \times I^2 \times R\cos\varphi = 0{,}599kW \tag{32}$$

$$\Delta V_{NYY} = \sqrt{3}(R\cos\varphi + X\sin\varphi)I = 0{,}82V \tag{33}$$

$$\%\Delta V_{NYY} = \frac{0{,}82}{400} = 0{,}21\% \tag{34}$$

2. NA2XY 1x240 mm^2 cable, resistance value 0.125 ohm/km and reactance 0.092 ohm/km

$$R = \frac{0{,}125}{1000} \times 50 = 0{,}00625\Omega \tag{35}$$

$$X = \frac{0{,}092}{1000} \times 50 = 0{,}00435\Omega \tag{36}$$

$$P_{losses-NA2XY} = \sqrt{3} \times I^2 \times R\cos\varphi = \sqrt{3} \times (225{,}34)^2 \times 0{,}00625 \times 0{,}89 = 0{,}489kW \tag{37}$$

$$\Delta V_{NA2XY} = \sqrt{3}(R\cos\varphi + X\sin\varphi)I = 0{,}78V \tag{38}$$

$$\%\Delta V_{NA2XY} = \frac{0{,}78}{400} = 0{,}2\% \tag{39}$$

The Main Circuit Breaker (MCB) serves as a safety protector. The MCB will disconnect the circuit when an overcurrent disturbance is detected. The MCB calculation based on GREI is 115% of FLA. The determination of the MCB are as follows.

1. Based on the consideration of a motor with a capacity of ≤15kW, using the SS method, the type chosen is Motor Protection Circuit Breaker (MPCB).
2. Based on considerations, even though the motor has a capacity of ≤15kW but uses the VFD method, the D curve class MCB was chosen because the MPCB is less responsive.
3. Based on the consideration of a motor with a capacity of ≥132 kW, using the soft starter method, the type chosen is MCCB 400A.

E. Power Factor Improvements

Reactive power compensation is an action to overcome the low power factor by installing capacitors so as to neutralize the effect of reactive power in an electric power system. Low power factors have the potential to cause disturbances in power quality to affect the system as a whole and even potentially damage installed equipment and systems. In this research, it has a large total reactive power, so the existing power factors are:

$$\cos\varphi = \frac{P}{S} = \frac{433{,}6}{496{,}12} = 0{,}873 \tag{40}$$

$$\tan\varphi_1 = \tan 0{,}507^\circ = 0{,}555 \tag{41}$$

The desired power factor is Cos φ2 = 0,98

$$\tan\varphi_2 = \tan 0{,}2003^\circ = 0{,}203 \tag{42}$$

$$Q_2 = \sqrt{(442{,}45)^2 - (433{,}6)^2} = 88{,}05kVAR \tag{43}$$

$$Q_C = P(\tan\varphi_1 - \tan\varphi_2) = 152{,}63kVAR \tag{44}$$

The installation of bank capacitors uses the mounting configuration on the side of the main low voltage busbar, rather than per load. This decision was chosen because all needs are concentrated at a single point known as reactive power distribution.

F. *Transformator Capacity*

Based on the calculated PLD of 496.12 kVA, multiplication is carried out with an expansion factor of 20% to determine the power capacity of the installed transformer, namely:

$$Transformator = Peak\ Load\ Demand \times 120\% = 595{,}34kVA \quad (45)$$

Referring to the catalogs of transformer on the market, the capacity of the chosen transformer is 630kVA.

G. *Comprehensive Study and Analysis*

Comprehensive analysis of the overall load rating reaches 534.5 KW, the selection of a 630 kVA transformer for a peak load of 496.12 KVA, with 2 conditions, namely:

1. Normal has a reactive power of 240.5 KVAR and a power factor of 0.873.
2. The design results have a reactive power of 80.05 KVAR and a power factor of 0.98.

The results of the power flow simulation show that the total power is 478kW, the reactive power is 243kVAR, the power factor is 0.8915 and the bus voltage is 387.8V in the normal system. Meanwhile, the total power is 476kW, the reactive power is 75 kVAR, the power factor is 0.9879, and the bus voltage is 391.5V in the system design.

By successfully contributing positively to improving the quality of voltage in the system bus as well as efforts to reduce reactive power and power loss. Figure 11 shows a representation of the maintenance diagram of the electrical power installation system based on feeder 01 are 8 groups of motors with VFDs. Figure 12 shows a representation of the maintenance diagram of the electrical power installation system based on feeder 02 there is 1 motor with VFD, 1 motor with soft starter and 8 motors. Figure 13 shows a representation of the maintenance diagram of the electrical power installation system based on feeder 03 consisting of 1 motor with VFD, 1 motor with soft starter and 8 motors. The power flow diagram of the electrical system comprehensively describes the input process from the PLN source to the load eventually.

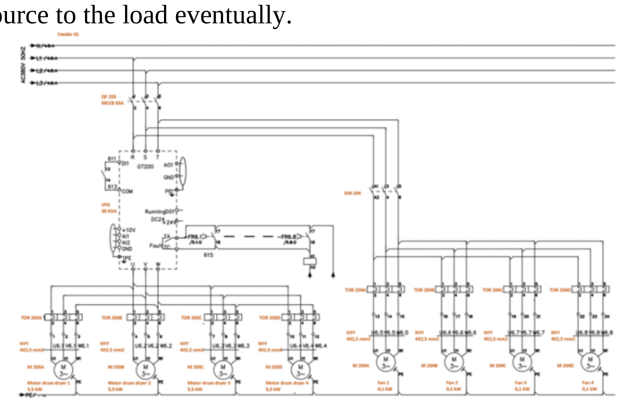

Fig. 11. *Feeder 01 wiring diagram*

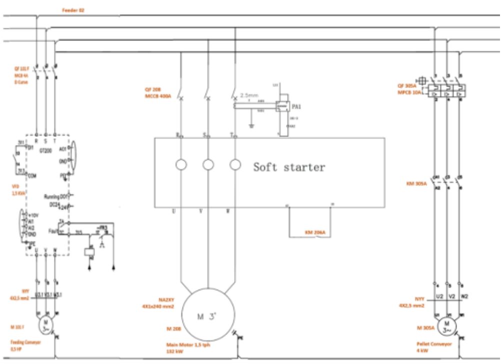

Fig. 12. *Feeder 02 wiring diagram*

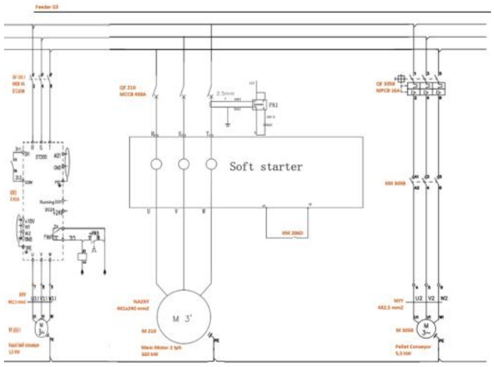

Fig. 13. *Feeder 03 wiring diagram*

H. *Energy Efficiency and Emission Reduction*

This design ensures that the power distribution system can operate with a high level of efficiency. By optimizing power distribution and load type, energy use can be maximized. The selection of equipment and system configuration are designed in such a way as to reduce power losses during the distribution process.

The result of this design has a transformer loading percentage of 76.5% from the power rating of a 630 kVA transformer. Thus, the transformer works well as it is still below 85% of capacity. Providing benefits both in terms of operational efficiency and service life. Compared to pre-optimization conditions, transformers work harder and create less efficient operating conditions and allow overloads to occur.

The total potential energy savings after the design reached 58,22kW. Referring to the estimated operational working hours for a year of 6000 hours, energy savings of 1253 kWh per year are obtained multiplied by emission factors to obtain emissions that can be reduced by:

$$E_{CO_{2e}} = Activity\ data \times Emission\ Factor = 303{,}90\ ton\ CO_{2e} \quad (46)$$

In a broader context, the equivalent value is also presented to understand this positive impact. The potential emission reduction of 303.90 tons of CO_2 per year is equivalent to the amount of greenhouse gas emissions that can be avoided from 162 tons of coal burning or 107 kilo liters of diesel consumption, as well as the equivalent value with the action of planting 8,350 trees for 3 years. This reflects the industry's responsibility to the principles of sustainability and attention to reducing global environmental impacts.

1. Equivalent value of coal combustion
   The calorific value (CV) of medium-quality coal according to national emission data is 18,7 TJ/Gg. The average carbon (C) content coefficient of coal burned for power plants is 27,4 kg Carbon per terajoule or 51.24%. The oxidized fraction (OF) is 100 percent.

$$Activity\ data = \frac{E_{CO_{2e}}}{CV \times C \times FO \times \frac{44}{12} \times 10^{-3}} = 161{,}75tons \quad (47)$$

2. Diesel fuel combustion equivalent
   The Calorific Value (CV) of diesel oil according to national emission data is 42.12 TJ/Gg. The carbon (C) content coefficient of burned diesel oil is 85% while its density (ρ) is 910 kg/m3. The oxidized fraction (OF) is 100 percent.

$$Activity\ data = \frac{E_{CO_{2e}}}{\rho \times C \times OF \times \frac{44}{12} \times 10^{-3}} = 107\ kilo\ liters \quad (48)$$

3. Tree planting equivalent

The rate at which carbon is absorbed by trees depends on several factors, including the growth characteristics of the tree species, the conditions in which the trees are planted, and the density of the tree's wood. Although variable, we can make a rough estimate of the amount of CO_2 absorbed. The process involves determining the total weight of the tree, the dry weight of the tree, and the carbon weight in the tree. For example, data from a 3-year-old Eucalyptus Grandis tree, growing 28.87 feet tall with a trunk diameter (D) of 2.64 inches, shows that the weight value of CO_2 absorbed in trees per year is 0.0364 tons of CO_2. Using this value, the number of trees planted for carbon sequestration is equivalent to 303.90 tons of CO_2 can be calculated as follows.

$$Activity\ data = \frac{E_{CO_{2e}}}{D^2 \times 0{,}25 \times 120\% \times H \times 72{,}5\% \times 50\% \times \frac{44}{12} : 2204{,}6} = 8350 \quad (49)$$

Conclusion

This study showed that the starting method with a soft starter succeeded in reducing the inflow significantly, from 1372 A to 765 A or an average current surge of 5.75 times to only 3.25 times of FLA. In addition, Variable Frequency Drive (VFD) testing showed that it successfully optimized motor performance by adjusting the speed when the load fluctuated, resulting in a power consumption savings of 56.22 kW. Power factor improvements also proved important, with the addition of capacitor banks reducing reactive power losses from 243 KVAR to 75 KVAR. The installed transformer capacity of 630 KVA, LVMDP circuit breaker 1,000A, and proper cable selection demonstrate the reliability of the system by overcoming active power loss from 4,091 kW to 3,352 kW. The design of the Electrical power installation system that has been carried out shows high efficiency and reliability in increasing voltage stability from 387.8 volts to 391.4 volts and decreasing transformer loading from 85.20% to 76.50%. In addition, this research contributes to the mitigation of greenhouse gas emissions with a potential reduction of approximately 303.90 tons of CO2 per year.

Acknowledgements

We would like to thank Universitas Mercu Buana and Universitas Presiden for the national collaboration research. hopefully this article will be published and become a consumption for scholars.

References

[1] N. Kumar and O. Buwa, "A Review on Reactive Power Compensation of Distributed Energy System," in *2020 7th International Conference on Smart Structures and Systems (ICSSS)*, Jul. 2020, pp. 1–6. doi: 10.1109/ICSSS49621.2020.9202249.

[2] S. Yang, H. O. Gao, and F. You, "Integrated optimization in operations control and systems design for carbon emission reduction in building electrification with distributed energy resources," *Adv. Appl. Energy*, vol. 12, p. 100144, 2023, doi: 10.1016/j.adapen.2023.100144.

[3] H. Luo, Y. Li, X. Gao, X. Meng, X. Yang, and J. Yan, "Carbon emission prediction model of prefecture-level administrative region: A land-use-based case study of Xi'an city, China," *Appl. Energy*, vol. 348, p. 121488, 2023, doi: 10.1016/j.apenergy.2023.121488.

[4] M. P. Thakre and N. Kumar, "Evaluation and Control Perceptive of VSM-Based Multilevel PV-STATCOM for Distributed Energy System," *MAPAN*, vol. 36, no. 3, pp. 561–578, 2021, doi: 10.1007/s12647-021-00481-x.

[5] N. Kumar, P. Wagh, D. Kolhe, P. Arane, and P. Kadlag, "Power quality improvement in distributed energy resources for EV charging using STATCOM," in *2022 1st International Conference on Sustainable Technology for Power and Energy Systems (STPES)*, Jul. 2022, pp. 1–4. doi: 10.1109/STPES54845.2022.10006548.

[6] F. Unibio, L. D. Pabon Fernandez, E. A. Caicedo, J. L. Diaz Rodriguez, and A. Pardo Garcia, "Design of a Self-adjusting Reactive Power Compensation Prototype for Residential Application BT - Applied Computer Sciences in Engineering," J. C. Figueroa-García, C. Franco, Y. Díaz-Gutierrez, and G. Hernández-Pérez, Eds., Cham: Springer Nature Switzerland, 2022, pp. 437–449.

[7] S. M. Al-Refai, "Starting Analysis of Three-Phase Squirrel Cage Induction Motors. Case Study: Oil Production Field in Libya," in *2023 IEEE 3rd International Maghreb Meeting of the Conference on Sciences and Techniques of Automatic Control and Computer Engineering (MI-STA)*, May 2023, pp. 117–123. doi: 10.1109/MI-STA57575.2023.10169599.

[8] Y. C. E. Jonathan and S. B. A. Kader, "Prospect of Emission Reduction Standard for Sustainable Port Equipment Electrification," *Int. J. Eng.*, vol. 31, no. 8, pp. 1347–1355, 2018, [Online]. Available: https://www.ije.ir/article_73254.html

[9] L. M. Silalahi, M. Rafi Indrawan, S. Budiyanto, D. Hanafi, A. Hamid, and D. Ronaldo, "Smart Home Control System Design using Internet of Things Based Energy Harvesting Technology," in *2024 IEEE 6th Symposium on Computers & Informatics (ISCI)*, Aug. 2024, pp. 43–48. doi: 10.1109/ISCI62787.2024.10667797.

[10] C. M. Coman, A. Florescu, and C. D. Oancea, "Improving the Efficiency and Sustainability of Power Systems Using Distributed Power Factor Correction Methods," *Sustainability*, vol. 12, no. 8, 2020, doi: 10.3390/su12083134.

[11] A. Paramonov, S. Oshurbekov, V. Kazakbaev, V. Prakht, and V. Dmitrievskii, "Investigation of the Effect of the Voltage Drop and Cable Length on the Success of Starting the Line-Start Permanent Magnet Motor in the Drive of a Centrifugal Pump Unit," *Mathematics*, vol. 11, no. 3. 2023. doi: 10.3390/math11030646.

[12] A. Faulkner, S. B. Tennakoon, M. Al-Tai, and S. Mackay, "Load flow, short circuit analysis and load point reliability for Data Centre power distribution networks," in *2018 IEEE Industry Applications Society Annual Meeting (IAS)*, 2018, pp. 1–8. doi: 10.1109/IAS.2018.8544490.

[13] D. Accordini, E. Cagno, and A. Trianni, "Identification and characterization of decision-making factors over industrial energy efficiency measures in electric motor systems," *Renew. Sustain. Energy Rev.*, vol. 149, p. 111354, 2021, doi: https://doi.org/10.1016/j.rser.2021.111354.

[14] A. De Almeida, J. Fong, C. U. Brunner, R. Werle, and M. Van Werkhoven, "New technology trends and policy needs in energy efficient motor systems - A major opportunity for energy and carbon savings," *Renew. Sustain. Energy Rev.*, vol. 115, p. 109384, 2019, doi: https://doi.org/10.1016/j.rser.2019.109384.

[15] L. M. Silalahi, S. Budiyanto, F. A. Silaban, I. U. V. Simanjuntak, A. D. Rochendi, and G. Osman, "Optimizing The Performance Of The Power Station Generator Space Lighting System Performance Based On Internet Of Things Using ESP32," in *2021 3rd International Conference on Research and Academic Community Services (ICRACOS)*, IEEE, Oct. 2021, pp. 219–224. doi: 10.1109/ICRACOS53680.2021.9702010.

[16] F. A. Silaban, A. G. Rolanda, L. M. Silalahi, and S. Budiyanto, "Solar Panel Drive Design Based Internet of Things," *CCIT (Creative Commun. Innov. Technol. J.*, vol. 16, no. 1, pp. 100–110, 2023, doi: https://doi.org/10.33050/ccit.v16i1.2363.

[17] S. Kucuk and A. Ajder, "Analytical voltage drop calculations during direct on line motor starting: Solutions for industrial plants," *Ain Shams Eng. J.*, vol. 13, no. 4, p. 101671, 2022, doi: https://doi.org/10.1016/j.asej.2021.101671.

[18] I. U. V. Simanjuntak, J. Haidi, R. F. A. Putra, and L. M. Silalahi, "Comparison of MPPT optimization methods for P&O and PSO solar panels to overcome partial shading," *Int. J. Electron. Telecommun.*, vol. 70, no. 4, pp. 1023–1029, Nov. 2024, doi: 10.24425/ijet.2024.152090.

[19] I. U. V. Simanjuntak, H. Heryanto, A. W. Dani, K. S. Salamah, L. M. Silalahi, and M. Marsuki, "Analysis Of Solar Power Public Street Lighting Optimization With Pvsyst Software In A Residential Complex Area," *Int. J. Electron. Telecommun.*, vol. 70, no. 3, pp. 743–749, 2024, [Online]. Available: https://ijet.pl/index.php/ijet/article/view/10.24425-ijet.2024.149604

[20] M. H. Mehraban Jahromi, P. Dehghanian, M. R. Mousavi Khademi, and M. Z. Jahromi, "Reactive Power Compensation and Power Loss Reduction using Optimal Capacitor Placement," *2021 IEEE Texas Power Energy Conf. TPEC 2021*, pp. 1–6, 2021, doi: 10.1109/TPEC51183.2021.9384963.

[21] A. Trianni, E. Cagno, and D. Accordini, "Energy efficiency measures in electric motors systems: A novel classification highlighting specific implications in their adoption," *Appl. Energy*, vol. 252, p. 113481, 2019, doi: https://doi.org/10.1016/j.apenergy.2019.113481.

[22] A. Hughes and B. Drury, *Electric motors and drives: fundamentals, types and applications*. Newnes, 2019.

[23] H.-C. Chuang, G.-D. Li, and C.-T. Lee, "The efficiency improvement of AC induction motor with constant frequency technology," *Energy*, vol. 174, pp. 805–813, 2019, doi: https://doi.org/10.1016/j.energy.2019.03.019.

[24] A. Abu-Jasser, H. El-Ghussain, and H. Mughari, "Power Flow Analysis of a 22/0.4kV Distribution Transformer Using ETAP Software Case Study: Al FAIROZ Residential Area in the Gaza City," in *2021 International Conference on Electric Power Engineering – Palestine (ICEPE- P)*, Mar. 2021, pp. 1–5. doi: 10.1109/ICEPE-P51568.2021.9423482.

[25] H. T. Dat, N. T. Bich Tuyen, L. Q. Binh, N. N. Phuc Diem, and L. T. Tinh Minh, "Evaluation and Improvement Distribution actual network Reliability using ETAP," in *2021 International Symposium on Electrical and Electronics Engineering (ISEE)*, Apr. 2021, pp. 193–198. doi: 10.1109/ISEE51682.2021.9418645.

[26] P. Bhase and M. Lathkar, "Energy conservation using VFD," in *2015 International Conference on Energy Systems and Applications*, Oct. 2015, pp. 531–536. doi: 10.1109/ICESA.2015.7503406.

[27] V. Kazakbaev, V. Prakht, V. Dmitrievskii, and D. Golovanov, "Feasibility Study of Pump Units with Various Direct-On-Line Electric Motors Considering Cable and Transformer Losses," *Applied Sciences*, vol. 10, no. 22. 2020. doi: 10.3390/app10228120.

[28] R. Saidur, S. Mekhilef, M. B. Ali, A. Safari, and H. A. Mohammed, "Applications of variable speed drive (VSD) in electrical motors energy savings," *Renew. Sustain. Energy Rev.*, vol. 16, no. 1, pp. 543–550, 2012, doi: https://doi.org/10.1016/j.rser.2011.08.020.

[29] M. Sequeira and S. Alahakoon, "Energy efficient variable speed drives empowered with torque estimation," *Energy Procedia*, vol. 160, pp. 194–201, 2019, doi: https://doi.org/10.1016/j.egypro.2019.02.136.

[30] A. Abdel Menaem, M. Elgamal, A.-H. Abdel-Aty, E. E. Mahmoud, Z. Chen, and M. A. Hassan, "A Proposed ANN-Based Acceleration Control Scheme for Soft Starting Induction Motor," *IEEE Access*, vol. 9, pp. 4253–4265, 2021, doi: 10.1109/ACCESS.2020.3046848.